On the Role of Successive Downstream Development in East Asian Polar Air Outbreaks[1]

CHANG HI JOUNG

Department of Meteorology, College of Natural Sciences, Seoul National University, Shinrim-Dong, Kwanak-Ku, Seoul, Korea

MATTHEW H. HITCHMAN

Department of Atmospheric Sciences, University of Washington, Seattle 98195

(Manuscript received 25 November 1981, in final form 7 June 1982)

ABSTRACT

A composite of 16 strong East Asian polar outbreak occurrences, widely separated in time, reveals a clear sequence of events: beginning over the western North Atlantic six or seven days in advance of the key day (as defined by the cold frontal passage over Korea) troughs and ridges are seen to form, develop and decay successively downstream of one another across the Eurasian continent until the polar outbreak occurs. These troughs and ridges reach their maximum amplitude in much the same location and at the same time relative to the key day in the majority of the 16 cases. The center of the wave packet moves along a curved trajectory approximating the mean 300 mb flow at a nearly constant rate of 30° longitude per day. The perturbation moves as an essentially barotropic dispersive wave across most of Eurasia, but its evolution becomes highly baroclinic as it approaches the East Asian coast. The wavetrain nature of this perturbation breaks down as it propagates out over the Pacific Ocean. This breakdown coincides in 8 of the 16 cases with the formation of a large amplitude ridge of great meridional extent.

1. Introduction

Several times during each winter season, a mass of cold Siberian air advances southeastward across the East Asian coast, accompanied by strong northerly winds, often causing natural disasters. The hope that these events might have a "typical" evolution upstream prompted this investigation. In order to discern common features in this class of extreme events, 16 such cases were chosen for compositing, each case consisting of a 13 day sequence beginning a week before the cold air outbreak.

The signal that emerges is strongly reminiscent of many cases of successive downstream development cited in the literature (Cressman, 1948; Hovmöller, 1949; van Loon, 1965). To better understand this fundamental dynamical process, the characteristics of this phenomenon and its relationship with East Asian polar air outbreaks, will be documented for purposes of comparison with existing theory. It is hoped that this will provide greater insight in interpreting forecast model output.

2. Compositing method and data

The surface synoptic situation involved in these polar outbreaks is characterized by an intense eastward-moving cyclone–anticyclone pair. In the wake of the cold front, a sharp east–west pressure gradient and north–south temperature gradient make for strong surface winds and a rapid drop in temperature. With this synoptic model in mind, we defined two criteria for including an event in the composite: a surface pressure gradient over Korea exceeding 2.5 mb $(100\ \text{km})^{-1}$ and a drop in daily mean surface temperature at South Korean stations of more than 5°C in one day. In addition, we required that the events selected be separated by at least 10 days. The 16 cases during the winters of 1965–75 which met these criteria are listed in Table 1. Each day of cold air outbreak as defined by the above criteria will hereafter be called the "key day" and assigned the position of day 8 in the composite.

Fig. 1 shows 24-hour composite temperature changes averaged for the 16 cases. Temperatures used are daily mean surface station data, averaged among five South Korean stations and the 16 cases for each day. The temperature is observed to remain nearly constant until near the key day, where it drops an average of 9°C from day 7 to 9, then rises the same amount from day 9 to 12.

National Meteorological Center Northern Hemisphere operational primitive equation model analyses of geopotential height and temperature at the 300, 500 and 850 mb levels for the 16 cases were arithmetically averaged for each of the 13 days extending

[1] Contribution No. 633, Department of Atmospheric Sciences, University of Washington, Seattle.

0027-0644/82/091224-14$07.50

TABLE 1. Key days for polar air outbreaks.

Case	Day 8
1	1200 GMT 15 Dec 1965
2	1200 GMT 10 Feb 1966
3	0000 GMT 30 Nov 1966
4	1200 GMT 14 Jan 1968
5	1200 GMT 18 Feb 1968
6	1200 GMT 4 Feb 1969
7	0000 GMT 26 Dec 1969
8	1200 GMT 4 Jan 1970
9	1200 GMT 12 Dec 1970
10	0000 GMT 4 Jan 1971
11	1200 GMT 28 Nov 1971
12	0000 GMT 12 Dec 1972
13	0000 GMT 6 Feb 1973
14	1200 GMT 21 Dec 1973
15	1200 GMT 23 Jan 1974
16	1200 GMT 20 Feb 1975

from 7 days before until 5 days after the key day. In each case the cold front was quite distinct on successive six-hourly surface analyses, so upper level data for 0000 or 1200 GMT were used in each case, depending on which time most closely followed the time of the cold frontal passage on the key day as indicated in Table 1. These composite maps are the basis for the results described in the next section.

3. Hemispheric composite maps

We will focus on the systematic alternating height rises and falls which are obviously related to events near the East Asian coast on day 8, while ignoring the weaker, less coherent features which are a reflection of sampling fluctuations. Fig. 2 shows 500 mb height two-day difference maps at intervals of two days, beginning with the change from day 2 to 4 (6 and 4 days, respectively, before the key day). Such difference maps tend to emphasize temporal fluctuations with periods on the order of twice the differencing interval (four-day periods, in this case). This sequence of maps reveals a train of alternating centers of rising and falling heights, propagating along a curved trajectory from 290°E (longitude 70°W) eastward to 190°E (longitude 170°W). The train is centered over the East Asian coast near the key day, day 8. Not shown are maps of other parameters[2] in which this phenomenon is also quite evident.

As indicated by the straight lines in Fig. 2, individual centers of rising and falling height (labeled A through H) retain their identity on several successive maps as they move downstream. The time continuity of these individual centers was confirmed on the basis of daily height and height change maps. A newly prominent center on a particular map is shown with no past movement, while the previous positions of an established center are marked with an x, as obtained from the previous odd-numbered (not shown) and even numbered two-day difference map.

It is evident that the "wave packet" associated with the cold air outbreak propagates downstream at a rate considerably faster than the movement of the individual 48-hour height change centers. This difference in phase speeds results in amplification of successive centers downstream of the wave packet and weakening of centers upstream.

Clear evidence for successive downstream amplification is also found in the difference maps for 850 and 300 mb height. The amplitude increases with altitude for each center on all the height difference maps. The two-day difference maps for the 500 and 300 mb levels give centers of rising and falling heights in very nearly the same locations. The 850 mb centers over the Atlantic on Figs. 2a, b and eastward of 100°E on Figs. 2c–e are displaced downstream by ⅛ to ¼ wavelength, relative to the corresponding 500 and 300 mb centers. The 850 mb centers are shown by primed letters (A′, B′, etc.) on Fig. 2, if they are distinguishable from the 500 mb centers. The main pattern is also discernible in the difference maps of temperature and thickness, but the amplitudes of such centers when the wave packet is in the vicinity of the coast of Asia are much larger than when the wave packet is west of that region (prior to the key day).

The trajectory along which the wave packet propagates is indicated by the heavy line shown on each map of Fig. 2. In the region of activity (290°E eastward to 190°E) the trajectory was chosen as the curve which best goes through the time-evolving locus of

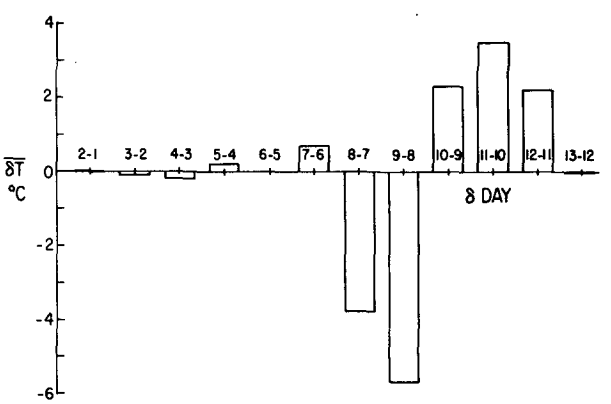

FIG. 1. 24 hour composite surface temperature changes in South Korea.

[2] Composite maps of the following quantities were compiled: daily 300, 500 and 850 mb values of geopotential height, temperature, vorticity, vertical shear of the zonal wind and height deviations from 1965–75 winter climatology; daily values of 300–500 and 500–850 mb thicknesses; one-, two-, and three-day difference maps of geopotential height, temperature and thickness; and an activity index for 300, 500 and 850 mb height, being the 12-map mean of the corresponding one-day difference magnitudes at each point. Also compiled were maps of height standard deviation among the 16 cases at each point on each day.

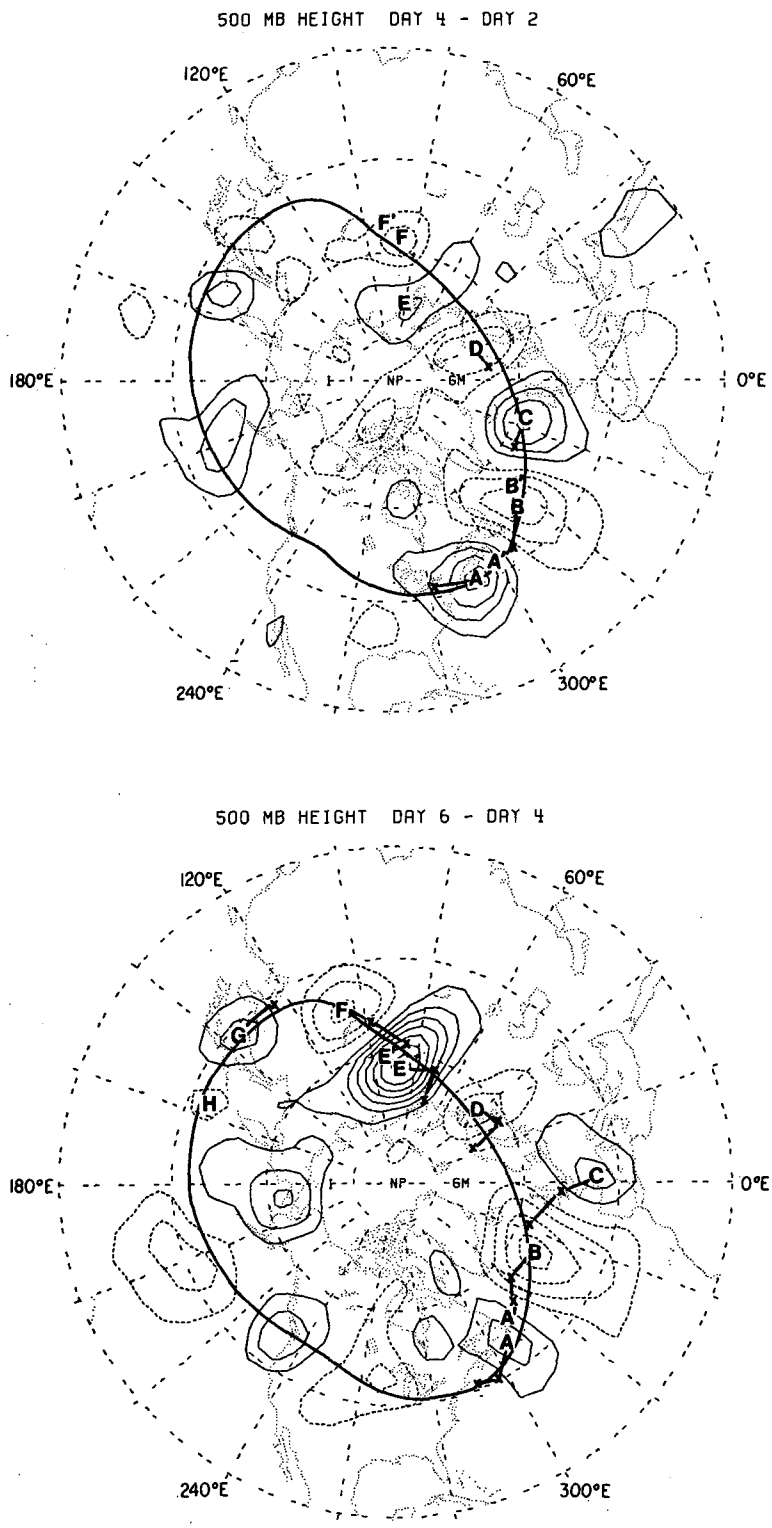

FIG. 2. Two-day difference maps of 500 mb height (contour interval 30 m). The zero contour has been omitted for clarity. Solid contours represent rises and dashed contours falls. Superimposed on each map is the trajectory chosen for use in Section 4. Each time-continuous height change center is labeled A through H, together with its past history. The position of the corresponding 850 mb centers are plotted as primed letters if they are in a noticeably different location.

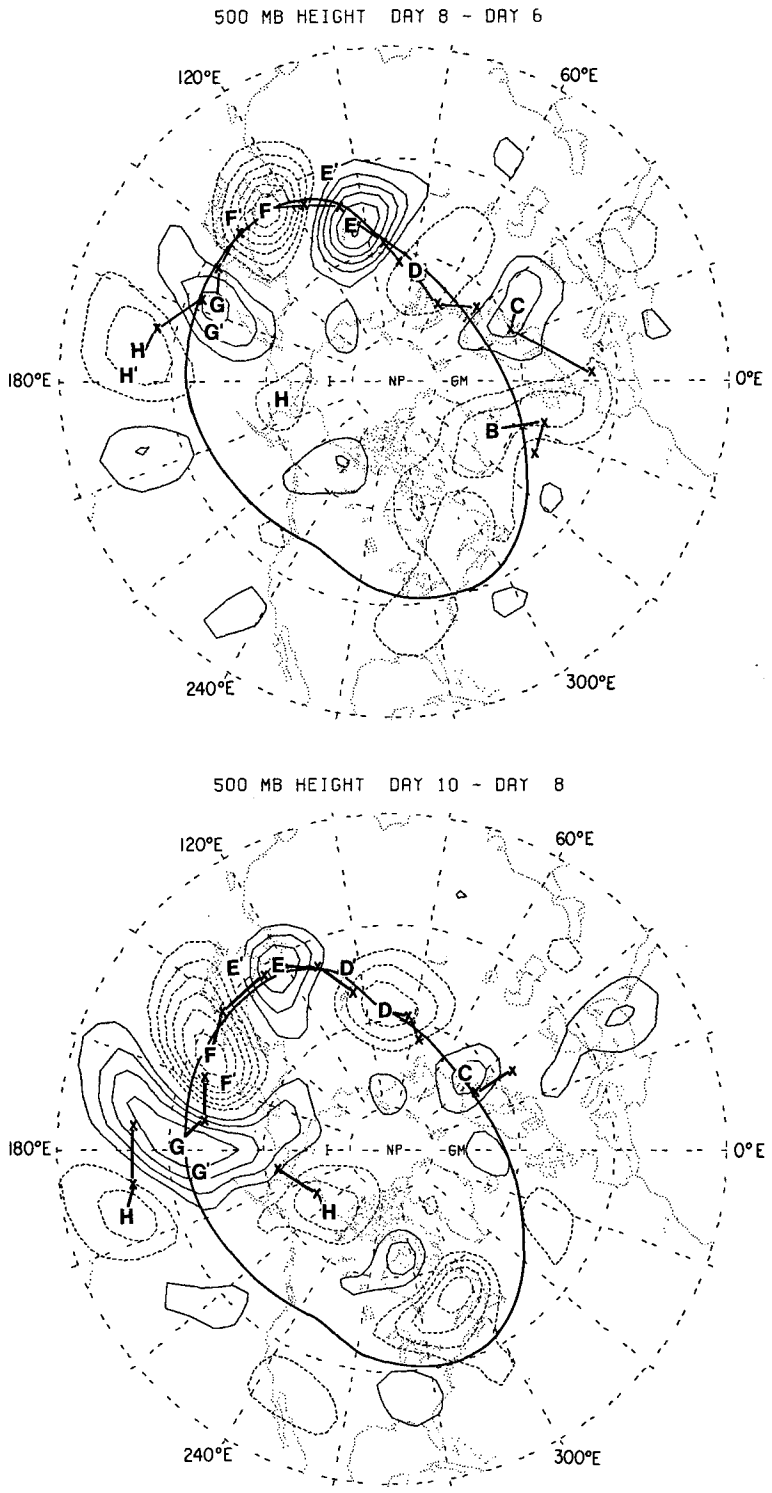

FIG. 2. (*Continued*)

largest height change centers at 500 and 300 mb. One might expect that the background flow pattern would influence the motion of the wave packet so that the trajectory would closely approximate height contours. Fig. 3 shows this trajectory superimposed upon the time mean 500 mb height map for the 13 days of the composite of 16 events. Evidently, there is a strong relationship, but since the trajectory goes

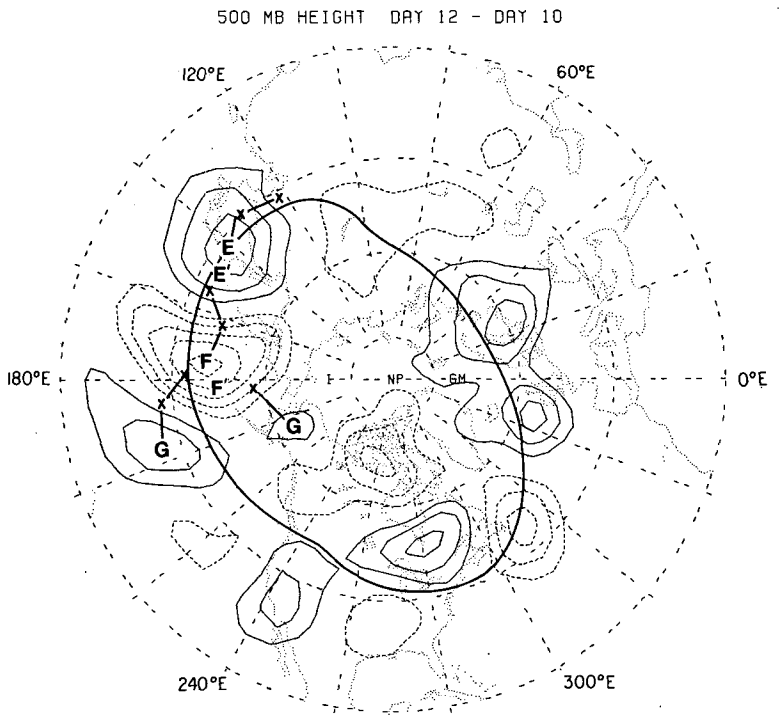

FIG. 2. (*Continued*)

through an evolving field of height change maxima, it would look somewhat different than height contours of a 13-day mean field. The trajectory through the height change centers was extended into the region of inactivity, 190°E eastward to 290°E, by approximately following the 5460 m contour of Fig. 3. It is this closed trajectory which is shown in Figs. 2 and 3 and is used in the time–longitude diagrams in the next section. It is extended into longitudes of inactivity to avoid features of interest being cut by figure margins in Section 4 and to provide a contrast of the wave train signal with random activity.

To illustrate the "typical" evolution of the flow pattern in these events, the composite 500 mb height maps on days 4, 6, 8 and 10 are presented in Fig. 4. To facilitate comparison with the tendency maps of Fig. 2, the two-day height change contours are superimposed (the day 4–day 2 height changes onto the resulting day 4, 500 mb map, etc.). The most prominent deviations from the time mean flow of Fig. 3 are highlighted with a trough or ridge axis. These composite troughs and ridges are also quite coherent in time and are labeled T1, R1, T2, R2, T3 and R3, in order of their appearance. For an indication of case-to-case variability, the axes of troughs and ridges in the individual cases which were clearly participating in the successive downstream development, as traceable in the individual case 500 mb map sequences, are plotted in the accompanying Fig. 5 for days 4, 6, 8 and 10. The flow evolution in each individual case had aspects which made it quite unique. No single case may be held as representative of the rest. Nevertheless, several common features may be described, as seen in the evolution of the composite flow.

Four days before the key day a prominent ridge (R1) can be seen over the eastern North Atlantic (Fig. 4a). Centers B and C indicate that it has been growing in amplitude and moving eastward for the previous 48 hours. The large trough over the western North Atlantic (T1) is seen to be between centers A and B, indicating movement toward the northeast with filling close upstream. Over Scandinavia, a second trough (T2) has been forming, as shown by center D, and there is already a ridging tendency just downstream, as suggested by center E. The corresponding map of positions in the individual cases for T1, R1, and T2 (Fig. 5a) shows that these features are common to nearly all the cases, even at this large distance upstream of Korea. One feature in Fig. 4 which will prove to be of some importance is the large stationary region of low heights over eastern Siberia, reflecting the extreme cold of the wintertime lower tropospheric air in that region.

By day 6 (Fig. 4b) T1 and R1 are no longer very noticeable and T2 has moved downstream somewhat. Due to the center of the wave packet propagating more rapidly than the individual troughs and ridges,

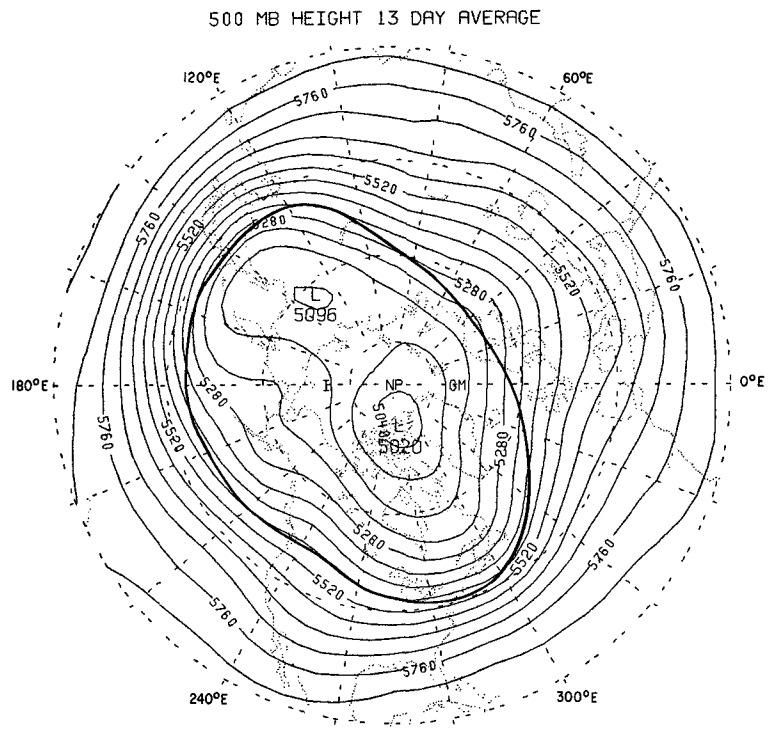

FIG. 3. Composite 13 day mean 500 mb map (contour interval 60 m), with the trajectory superimposed.

center E is now the most prominent height change feature. The resultant large amplitude ridge (R2) exhibits substantial southwest–northeast tilt. Center F indicates the formation of the short-wave trough (T3) on the southwest side of the Siberian low by two days before the key day. In Fig. 4c, centers E and F show the marked amplification of the ridge and trough pair (R2 and T3) as they move southeastward toward the coast to their positions as seen on the key day. The surface anticyclone–cyclone pair preceding R2 and T3 by ~¼ wavelength (not shown) causes the polar outbreak. The pre-existing large stationary low is seen to be essential in adding sufficient meridional extent to the propagating trough (T3) such that the main flow on the day 8 500 mb map is diverted as far south as 35°N. Many individual trough axes clearly extend down to 20°N (Fig. 5c).

This strong amplification and increased meridional extent of T3 by day 8 marks a change in the flow evolution from what it was prior to the key day. A split in the propagation appears to occur, with subsequent activity to the northeast and southeast. (Note split centers H and G in Figs. 2d, e.) On day 10 (Fig. 4d) the resulting southeast–northwest tilting ridge (R3), north of 40°N near 180°E, and the trough downstream are seen to have a large latitudinal extent. Successive downstream development is not observed eastward of the central Pacific. The uniform propagation of a single wave packet across Eurasia is radically altered upon passing over the coast.

Since there is a strong suggestion of blocking activity occurring after the key day over the Pacific in the composite fields, the 16 individual cases were investigated to see whether the end of successive downstream amplification might be linked with the onset of blocking. Twice-daily 500 mb charts on microfilm were examined for days succeeding the key day for each case and instances of blocking and transient ridges were objectively evaluated. The criteria of Hartmann and Ghan (1980) were adapted as follows.

In the longitude band 140°E–140°W, 500 mb heights along the 55°N latitude line were compared with the wintertime mean heights along that line (the wintertime mean being that of the ten 120-day winter seasons beginning on 15 November 1965, from which the 16 cases were chosen). If the 500 mb geopotential height for some individual day exceeded the mean for some point along this line by 250 m or more for at least one day, then a case of ridging was initiated. The case was then continued until the movement in any 12 h period was more than 10° longitude, until the total movement was more than 10° longitude, or until the height became less than the critical value. The critical value at 55°N, 180°E, for example, is 5450 m. Ridges lasting six days or more are blocking ridges, otherwise they are termed transient ridges.

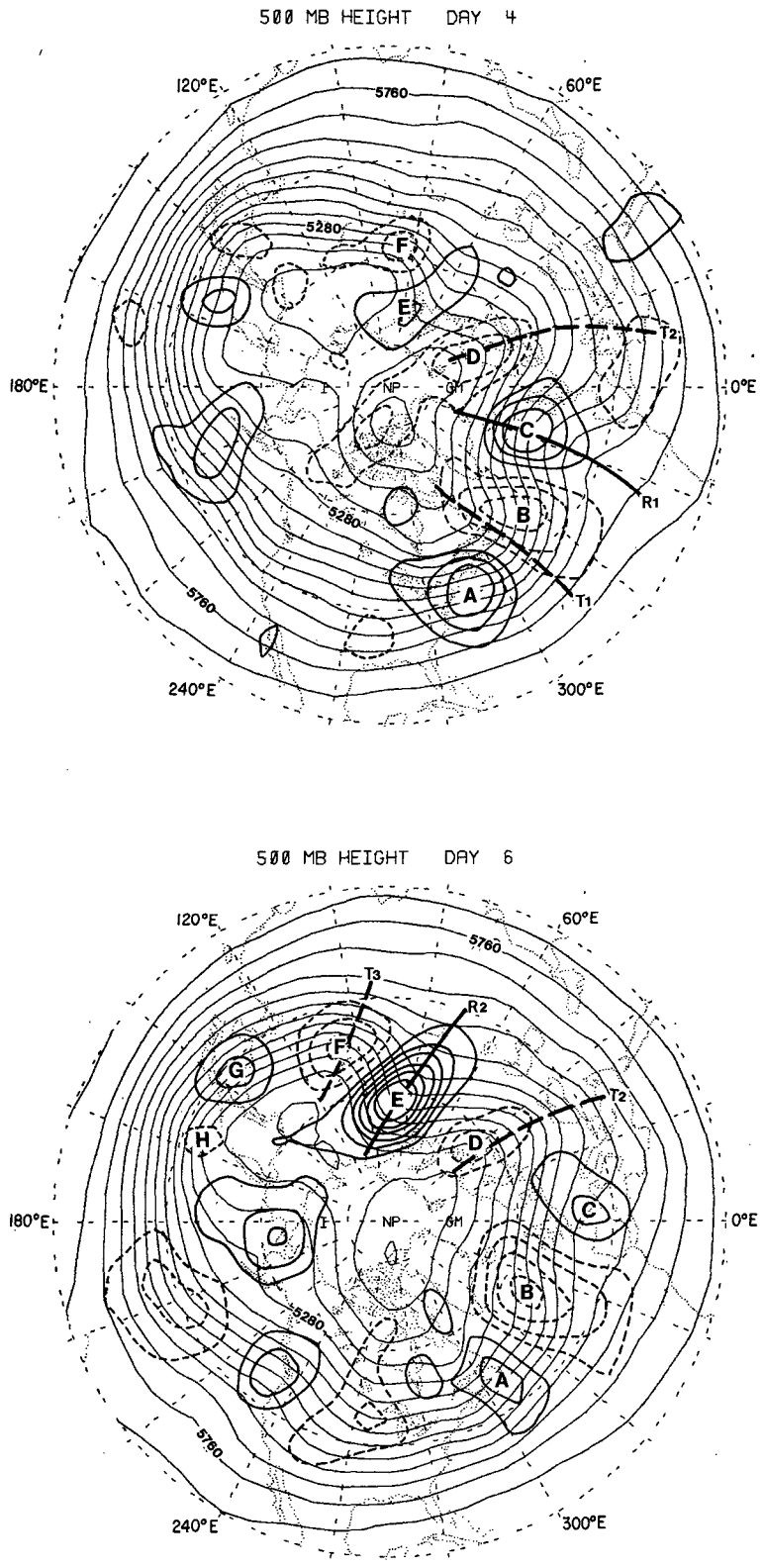

FIG. 4. Day 4, 6, 8 and 10 500 mb composite height maps (contour interval 60 m). Superimposed are the corresponding previous 48-hour height change centers from Fig. 2. Ridge axes are marked with heavy solid lines, trough axes with heavy dashed lines.

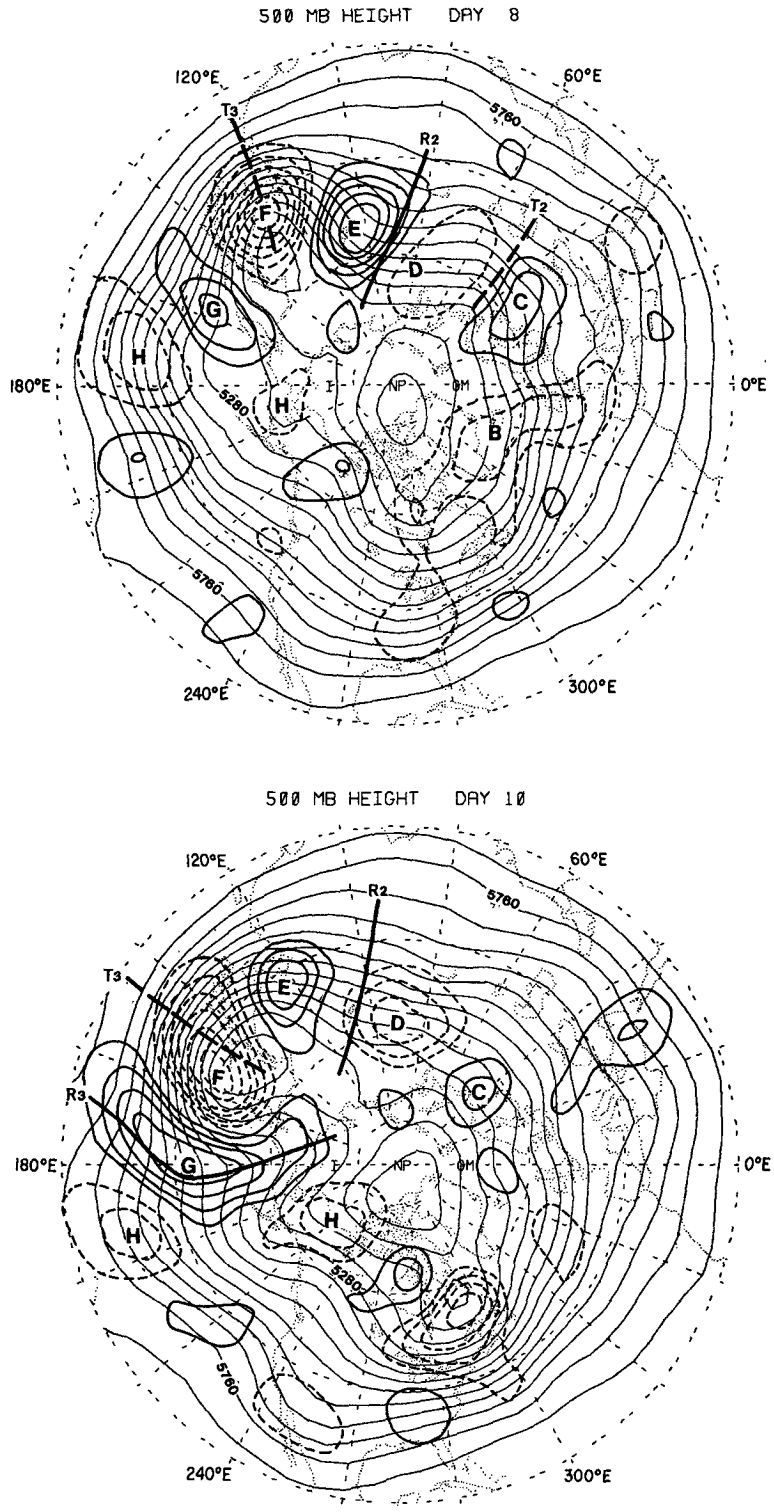

FIG. 4. (*Continued*)

In fully half of the 16 cases, a large-amplitude ridge exceeding the critical value formed after the key day over the Pacific. Table 2 lists these cases (as numbered in Table 1), together with the duration, maximum amplitude and central longitude of each ridge. Cases 3 and 10 meet Hartmann and Ghan's stringent qual-

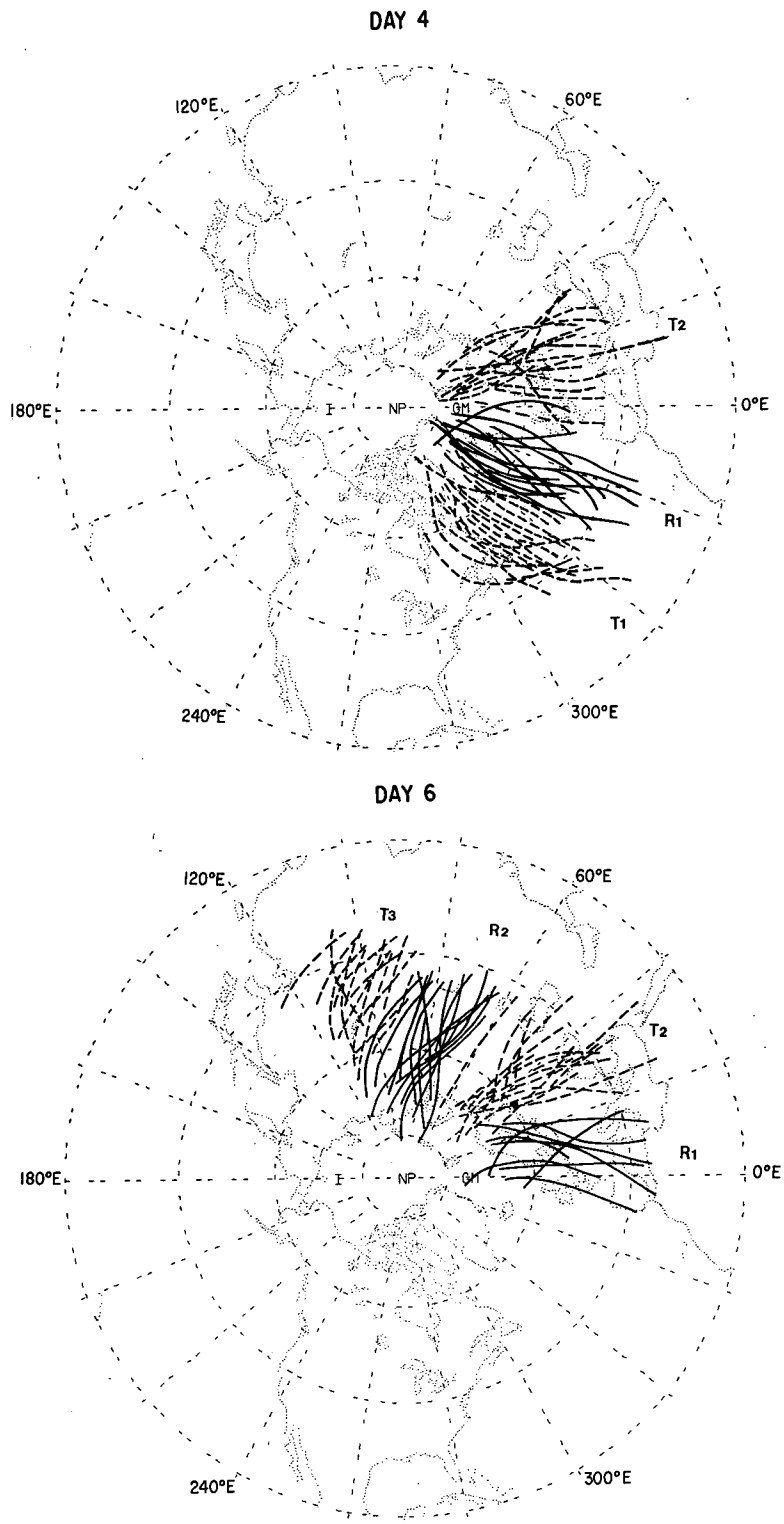

FIG. 5. Trough (dashed line) and ridge (solid line) axes in the 16 individual cases for days 4, 6, 8 and 10, labeled in order of their appearance.

ifications for a blocking ridge. In their classification, a ridge becomes a strong block if the maximum amplitude exceeds the wintertime mean by 500 m. This corresponds to 5740 m at 55°N, 180°E. Thus in case 3 there is a strong block in the Pacific after the key day.

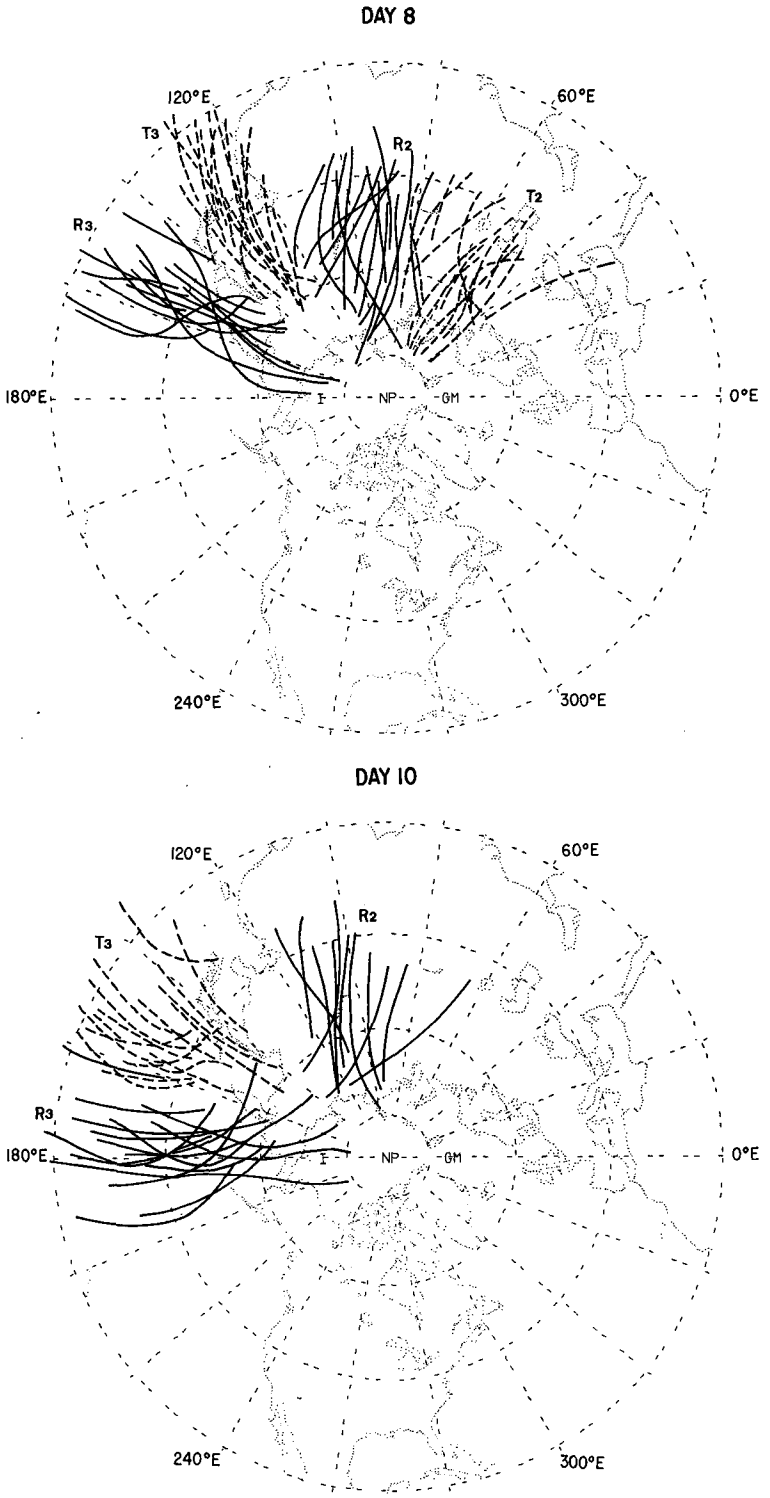

FIG. 5. (*Continued*)

4. Group propagation calculations

The trajectory specified in Section 3 is used as a tool to isolate the succession of anomalies from the background flow and to compare properties such as their relative amplitudes, lengths and phase speeds as they vary over the 13 day period. The traditional trough-and-ridge diagram, or Hovmöller diagram, is

TABLE 2. Cases of large-amplitude ridges over the Pacific after the key day.

Case number	Duration (days)	Maximum amplitude (m)	Central longitude
2	3.5	5680	160°W
3	7.0	5830	175°W
4	4.5	5600	180°E
6	2.5	5480	175°E
10	10.5	5670	165°W
11	2.5	5470	180°E
12	4.5	5700	180°E
15	5.0	5480	175°E

used in modified form in this section in order to show these features succinctly. In Hovmöller's original method, geopotential heights of the 500 mb surface at 35, 40, 45, 50, 55 and 60°N are averaged together at every fifth degree of longitude and plotted on the horizontal axis. Time increases downward and the values are contoured and shaded. Fig. 1 in Hovmöller (1949) and Fig. 11 in van Loon (1965) are excellent examples. They suggest that successive downstream development is a common phenomenon in the Northern Hemisphere winter and in both summer and winter in the Southern Hemisphere.

In preparing the time–longitude sections shown in Figs. 6 and 7, several changes have been made from the original method in order to more clearly present the data. Instead of an average over a latitude band, only the value linearly interpolated to the trajectory from the adjacent grid points is used. Since the trajectory crosses a wide range of latitudes, actual distance varies along the abscissa. The total trajectory length is 24 900 km, thus 5° of longitude equals approximately 340 km in these sections (as small as 220 km at 67°N and as large as 413 km at 42°N). Geopotential height and thickness values are contoured, where the 13 day mean value at each point on the trajectory has been subtracted out for each day so that amplitudes of the various positive and negative anomalies in the wave packet can be meaningfully compared. The resulting values of relative amplitudes were found to be rather insensitive to the exact choice for the trajectory. Various trajectories were tested with the result that if they fell within 5° of latitude of the trajectory used here, the values in Figs. 6 and 7 remained much the same, except for the amplitude of R3 at 850 mb near day 9.

The 300, 500 and 850 mb height time–longitude sections in Fig. 6 illustrate the successive downstream development evident from ~290°E eastward to ~190°E. While it is striking at all three levels, the amplitude increases with height. The axis of each of the six major positive or negative anomalies at 300 mb on Fig. 6 is copied onto each other section in Figs. 6 and 7 for purposes of phase comparison. West of about 60°E the features at 300 and 500 mb are nearly vertically aligned with those at 850 mb, but farther east R2, T3 and R3 are almost in quadrature with the corresponding high or low at 850 mb. The strong upstream tilt with height of the cyclone–anticyclone pair in the latter region is indicative of a strongly baroclinic structure, in contrast to the essentially barotropic structure further west. The increasing baroclinicity of the system as it propagates eastward toward the coast of Asia is also revealed in the thickness patterns (Fig. 7). Between 340 and 60°E there is very little activity in the thickness fields. There appears to be some indication of baroclinic activity in the thickness fields for T1 and R1 over the western North Atlantic. Corroborating evidence comes from Fig. 2a where we saw that west of ~70°E the 850 and 500 mb centers were in phase, with the exception of a slight upstream tilt with height of T1 and R1 (A, A′, B, B′) over the Gulf Stream. On the other hand, centers E, E′, F, F′, G, G′, H, H′ in Figs. 2c–e show substantial upstream tilt with height of R2, T3 and R3. Figs. 7a, b correspondingly show R2, T3 and R3 at 300 mb to lie over warm, cold and warm air, respectively.

These time–longitude sections clearly reveal the distinction between the phase propagation of individual positive or negative anomalies and the rate of propagation of the wave packet. The spatial extent of the wave packet is more accurately portrayed in Figs. 6 and 7 than in Fig. 2 since representing a moving set of waves by two-day differencing will spread the pattern out. At any given time the wave packet consists of about three individual centers, spanning about 120° of longitude. The lifetime of the individual centers is ~5 days, whereas the wave packet retains its identity for at least 11 days.

Anomaly maps of geopotential height departures from 1967–75 winter climatology were used to obtain an estimate of the horizontal wavelength L_s, corresponding to each of the six anomalies on the day that each in turn reaches its maximum amplitude in the composite. L_s is taken to be twice the along-trajectory diameter of the anomaly of interest at the 300 mb level. Estimates of this parameter, together with estimates of the following parameters based on the 300 mb time–longitude section, are presented in Table 3: k^* is the nondimensional zonal wavenumber, estimated from the relation $k^* = 2a\pi \cos\bar{\phi}/L_s$, where a = 6367 km and $\bar{\phi}$ is the average latitude of the center; c is the zonal phase speed of each individual wave, obtained from using the slope of the 300 mb anomaly axes shown by dashed lines in Fig. 6 in the relation $c = a\cos\bar{\phi}\Delta\lambda/\Delta t$; $\bar{\phi}$ and $\bar{\lambda}$ are the mean latitude and longitude of the center of the wave train, the longitude on a given day being estimated by connecting the points of maximum amplitude on Fig. 6 with a straight line, the latitude being the corresponding position on the trajectory of Fig. 2; G_x and G_y are the

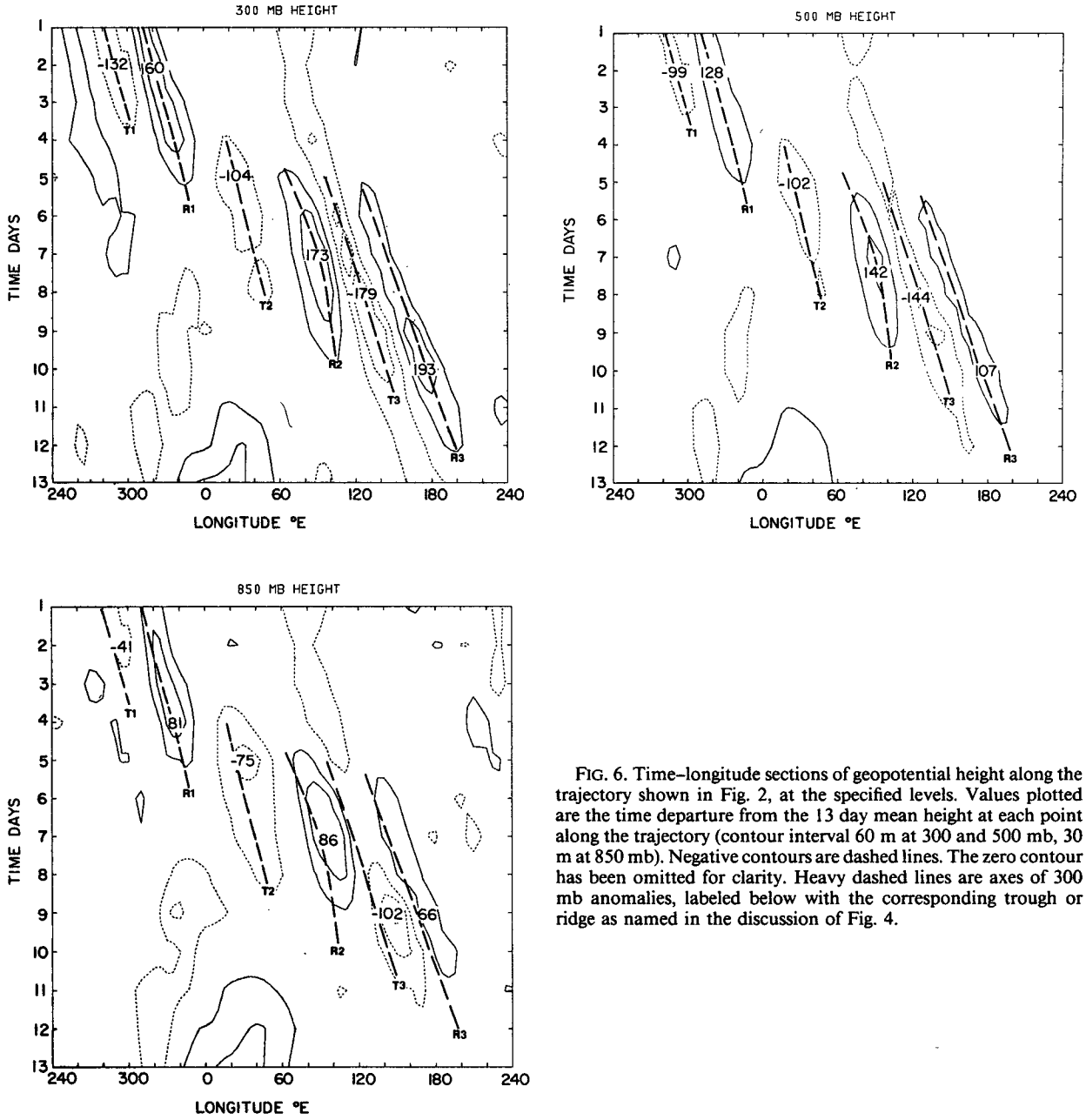

FIG. 6. Time–longitude sections of geopotential height along the trajectory shown in Fig. 2, at the specified levels. Values plotted are the time departure from the 13 day mean height at each point along the trajectory (contour interval 60 m at 300 and 500 mb, 30 m at 850 mb). Negative contours are dashed lines. The zero contour has been omitted for clarity. Heavy dashed lines are axes of 300 mb anomalies, labeled below with the corresponding trough or ridge as named in the discussion of Fig. 4.

zonal and meridional group speeds of the wave packet obtained from the slope of the line connecting the centers, corrected to the appropriate latitude, and from centered time differencing of $\bar{\phi}$, respectively.

The mean wavelength of the individual waves is 5400 km, while the mean wavenumber is 4.5. k^* decreases following the group's movement through higher latitudes and increases again for waves in the packet which move southeastward just before the key day. L_s remains fairly constant from wave to wave.

The six individual anomalies move eastward at rather slow speeds, in the range 4–11 m s^{-1}. The wave train moves eastward at a nearly constant rate of 30° of longitude per day or in the range 16–30 m s^{-1}.

By inspecting Fig. 6 we see that the amplitudes of T1 and R1 are somewhat larger than that of T2, while the amplitudes of R2, T3 and R3 are much larger than that of T2. (The amplitude of R3 at 850 mb on day 9 is actually ~90 which is the value obtained when the trajectory is chosen to go through the center G′ of Fig. 2). One might expect that the compositing method itself would cause amplitudes to decrease with increasing time and distance away from the key day and location, due to irregular wave spacing from

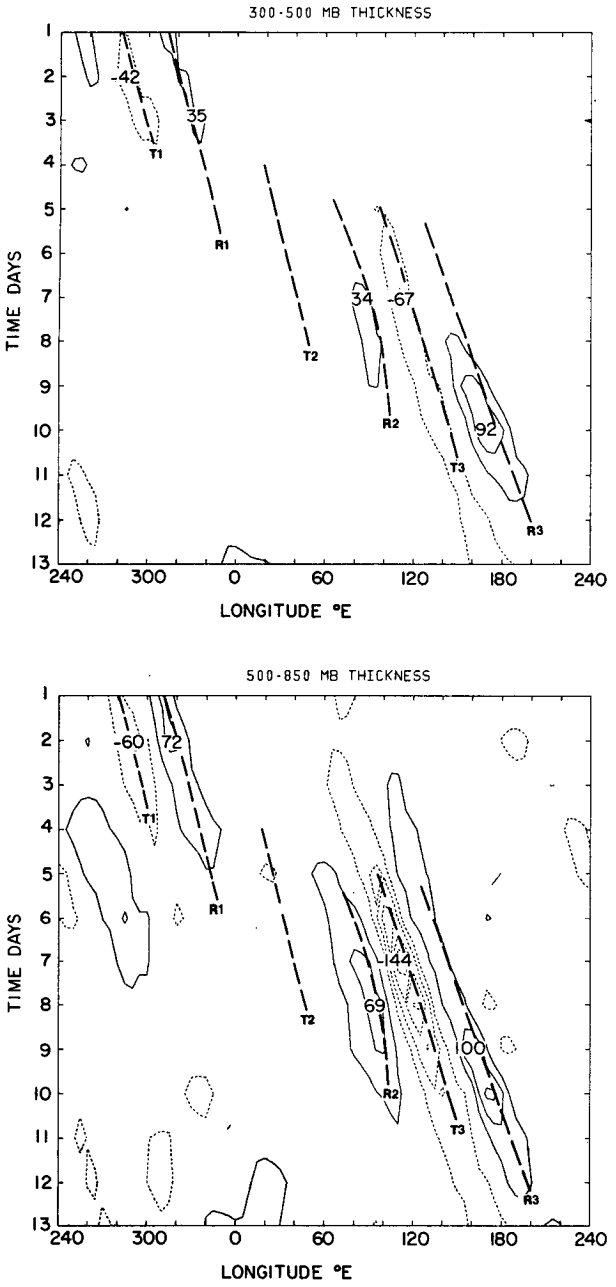

FIG. 7. As in Fig. 6, except time–longitude sections of upper and lower tropospheric thickness departures along the trajectory of Fig. 2 (contour interval 30 m).

case to case and the destructive interference which would result. Thus it is remarkable that the signal is as strong as it is, particularly over the Atlantic, far from the east coast of Asia. The locations where we find composite waves having upstream tilt with height and larger amplitudes is in qualitative agreement with known regions of strong baroclinicity (Blackmon *et al.*, 1977). Fig. 5 shows the spacing between waves to be quite regular from case to case and from day to day. This helps to explain the observed strength of the signal and may suggest that the development mechanism has a preferred length scale.

5. Discussion

We have found that East Asian polar outbreaks are frequently associated with wave packets which propagate eastward at 30° longitude per day along a trajectory which resembles a wintertime mean mid- or upper-tropospheric geopotential height contour. When a large number of individual cases are composited, the wave packet is first detectable over the western North Atlantic six or seven days before the outbreaks. However, in practice, it is not generally possible to identify an incipient cold air oubreak so far in advance of its occurrence. The individual troughs and ridges grow and decay, each being a temporary member of the larger unit, with trough and ridge pairs having a wavelength of ~5000 km throughout the group's evolution. It has also been shown that as the wave packet traverses the region west of ~60°E, the waves are equivalent barotropic in structure with amplitude increasing with height up to the 300 mb level. In contrast, after the wave packet moves east of ~60°E the waves acquire a vertical structure indicative of baroclinic development. In Figs. 4b, c, 5b and c, R2 exhibits marked southwest–northeast axis orientation in a region where $\partial\bar{u}/\partial y < 0$. Here eddy kinetic energy may be expected to increase at the expense of that of the mean flow by barotropic processes. We leave to others the difficult task of reconciling these observations with theory. But two mechanisms by which successive downstream development may occur are worth considering.

One such mechanism in which successive downstream development evolves from a localized initial perturbation has been elucidated by Simmons and Hoskins (1979) on the basis of numerical experiments with a hierarchy of models. It was diagnosed as being essentially a baroclinic phenomenon, the mechanism involving vortex stretching and shrinking adjacent to the initial local perturbation. Even in their Eady basic state model, where $\beta = 0$, a train of Rossby waves readily formed by the successive growth of new perturbations on the upstream and downstream edges of the train. The development patterns in their model runs are quite similar to what occurs in the composite data, except that the zonal extent of the model wave packet steadily increases with time, partly due to upstream development. The composite wave train appears to spread out near the key day in Fig. 6, but not before.

The second possibility, particularly for disturbances west of ~70°E, is that the downstream development is a manifestation of group velocity for barotropic waves. The average difference in eastward propagation speed between the group velocity of the

TABLE 3. Composite data parameter estimations: trough or ridge "wavelength" L_s; nondimensional zonal wavenumber k^* and phase speed c: central latitude and longitude of the wave packet $\bar{\phi}$ and $\bar{\lambda}$, and its zonal and meridional group velocity, G_x and G_y; and the difference in zonal propagation speed $G_x - c$.

Day	1	2 T1	3 R1	4	5 T2	6	7 R2	8 T3	9	10 R3
L_s (km)		5300	5300		5200		5700	5800		5200
k^*		5.5	4.5		3.1		3.6	5.0		5.5
c (m s^{-1})		7	7		4		5	9		11
$\bar{\phi}$ (°N)	44	42	53	58	66	66	59	43	42	44
$\bar{\lambda}$ (°E)	261	292	323	354	25	56	87	118	149	180
G_x (m s^{-1})	29	30	24	21	16	16	21	29	30	29
G_y (m s^{-1})		7	10	9	5	−5	−15	−11	1	2
$G_x - c$		23	17		12		16	20		18

wave packet and the phase speed of individual disturbances is ~ 18 m s^{-1}. This is reasonably consistent with the difference expected for a barotropic Rossby-Haurwitz wave on a β-plane:

$$G_x - c = (2\beta/k^2)[1 + (l^2/k^2)]^{-2},$$

where k and l are the zonal and meridional wavenumbers of the observed disturbances (see, e.g., Longuet-Higgins, 1964). The latitudinal dependence of β in this equation is of the right magnitude to account for the along-trajectory variation of $G_x - c$ (shown in Table 3). In such barotropic systems the mechanism for downstream development is the β effect. Meridional winds near the fringes of a prominent vorticity center will tend to induce the growth of a vorticity center of the opposite sign downstream, but tend to suppress such development upstream.

The troposphere cannot usually be neatly described as either barotropic or baroclinic. In order to model the observed waves it may be necessary to blend barotropic and baroclinic theories of successive downstream develoment.

These results provide an objective confirmation of some of the relationships which operational forecasters in East Asia have developed over the past few decades as a basis for predicting cold air outbreaks. Such forecasters are accustomed to looking far upstream to eastern Europe for the first signs of wave amplification. Our colleague, Lin Ben-Da, has recently performed an analogous compositing study of cold air outbreaks over eastern North America and did not find evidence of a well defined pattern of downstream development. Evidently, the dynamical processes which lead to cold air outbreaks over North America are more varied or more localized in time and space or both.

Acknowledgments. We thank Professors J. M. Wallace and C. B. Leovy for many helpful discussions and suggestions and Dr. G. H. White for help in using the NCAR computer facility. The National Center for Atmospheric Research is sponsored by the National Science Foundation. MHH's research was supported by the National Aeronautics and Space Administration under Contracts NASI-14341 and NS6-7805.

REFERENCES

Blackmon, M. L., J. M. Wallace, N.-C. Lau and S. L. Mullen, 1977: An observational study of the Northern Hemisphere wintertime circulation. *J. Atmos. Sci.*, **34,** 1040–1053.

Cressman, G. P., 1948: On the forecasting of long waves in the upper westerlies. *J. Meteor.*, **5,** 44–57.

Hartmann, D. L., and S. J. Ghan, 1980: A statistical study of the dynamics of blocking. *Mon. Wea. Rev.*, **108,** 1144–1159.

Hovmöller, E., 1949: The trough-and-ridge diagram. *Tellus,* **1**(2), 62–66.

Longuet-Higgins, M. S., 1964: On group velocity and energy flux in planetary wave motions. *Deep-Sea Res.*, **11,** 35–42.

Simmons, A. J., and B. J. Hoskins, 1979: The downstream and upstream development of unstable baroclinic waves. *J. Atmos. Sci.*, **36,** 1239–1260.

van Loon, H., 1965: A climatological study of the atmospheric circulation in the Southern Hemisphere during the IGY, part I: 1 July 1957–31 March 1958. *J. Appl. Meteor.*, **4,** 479–491.